RSC Advances

ROYAL SOCIETY OF CHEMISTRY

www.rsc.org/advances

Journal Name

ARTICLE

Anticorrosive Assay-Guided Isolation of Active Phytoconstituents from *Anthemis pseudocotula* Extracts and a Detailed Study of Their Effects on the Corrosion of Mild Steel in Acidic Media

Received 00th January 20xx,
Accepted 00th January 20xx

DOI: 10.1039/x0xx00000x

www.rsc.org/

H. Z. Alkhathlan*, M. Khan, M. M. S. Abdullah, A. M. AlMayouf, A. Yacine Badjah-Hadj-Ahmed, Z. A. ALOthman, A. A. Mousa

In this study, anticorrosive properties of various extracts (methanolic, aqueous methanolic and water extracts) of *Anthemis pseudocotula* for mild steel in 1.0 M HCl media is screened for the first time. Among the various tested extracts, methanolic extract of *A. psedocotula* shows highest corrosion inhibition activity. Anticorrosive assay-guided isolation of this methanolic extract results in the isolation of a highly potent anticorrosive compound, **APB** (luteolin-7-O-*β*-D-glucoside). The anticorrosive effects of **APB** on mild steel in 1.0 M HCl media were evaluated in details using gravimetric, Tafel plots, linear polarization, electrochemical impedance spectroscopy and SEM and EDS techniques. Tafel plots reveal that **APB** acts as a mixed-type inhibitor. The adsorption behaviour of this green inhibitor on the mild-steel surface obeys the Langmuir adsorption isotherm. Surface morphology study through SEM and EDS analysis display a noteworthy upgraded surface morphology of the mild steel plate in the presence of green inhibitor in 1.0 M HCl media. The results obtained from electrochemical tests and weight loss measurements are in good agreement which shows excellent inhibition efficiency for the natural compound **APB**.

Introduction

Corrosion is a common problem for several metals. In industries, it creates several major problems because of its perilous nature on metals.[1] The damage done by corrosion engenders more costs for the examination, renovation and replacement of various equipment and constitutes serious public and environmental risks. Corrosion of metals cannot be completely stopped, but it can be drastically reduced using various approaches, such as upgrading the materials,

[a] Department of Chemistry, College of Science, King Saud University, P.O.Box 2455, Riyadh - 11451, Saudi Arabia. E-mail: khathlan@ksu.edu.sa; Tel: +966-1-4675910, Fax: +966-1-4675992.

blending production fluids, process control and using chemical corrosion inhibitors.[2] Among these methods, the use of chemical corrosion inhibitors is usually the most suitable, practical and economical approach to accomplish this goal.[3] Several synthetic molecules have been reported as valuable corrosion inhibitors for metals.[4, 5] However, most of them are expensive and extremely toxic to human being and the environment. The toxicity of synthetic compounds and uncompromising environmental directives have led to the use of natural products as safe and effective green corrosion inhibitors.[6-8]

Natural products have the advantage of being biodegradable in nature, renewable, easily accessible, economical and, most importantly, are environmental friendly. Recently, several natural products, particularly plant extracts, have been reported to be an excellent, environmentally benign and economical source of corrosion inhibitors.[9-11] The extracts of various plants and their parts (leaves, fruits, roots, etc.) have been reported to possess commendable corrosion inhibition properties for metals in various corrosive media.[12-15] For example, the reported plant extracts with promising corrosion inhibitive properties include *Zenthoxylum alatum,*[9] *Phyllanthus amarus,*[13] *Uncaria gambir,*[10] *Strychnos nux-vomica*,[16] *Murraya koenigii*,[7] *Schinopsis lorentzii*,[17] *Phragmites australis*,[14] *Brugmansia suaveolens*, *Cassia roxburghii*,[11] *Polycarpaea corymbosa* and *Desmodium triflorum*.[15]

Although several plant extracts have been described to be prominent corrosion inhibitors for metals in different corrosive media, it has been well established that the inhibitive actions of plant extracts originate from the mixture of organic molecules in their composition. The organic molecules that are responsible for corrosion inhibitive actions have not been isolated and identified in most scientific investigations on green corrosion inhibitors [6,7,10,11,14,17]. Therefore, as part of our ongoing investigations on Saudi Arabian plants for the advancement of products of potential economic values,[18,19] we report here for the first time the corrosion inhibitive action of *Anthemis pseudocotula* extracts and anticorrosive assay guided isolation of the most active phytoconstituent that is responsible for the corrosion inhibitive properties of the extract.

Anthemis L. is one of the largest genera of the Compositae family, which is composed of approximately 210 species that are distributed in the Mediterranean region, southwest Asia, and some parts of eastern Africa.[20] In the flora of Saudi Arabia, approximately 17 species of *Anthemis* have been recorded, six of which are known to be widely distributed plant species in Saudi Arabia, whereas three have been identified to be endemic to Saudi Arabia.[21,22] *A. pseudocotula* Boiss is a semi-prostrate densely leafy annual herb with bright dark green feathery leaves and white flowers, which are 2 cm wide. This plant is among the most abundantly distributed plant species of the genus *Anthemis*.[22-24]

Experimental section

Collection and identification of plant material

The entire plant of wild growing *A. pseudocotula* was collected from Rowdah Khuraim, the Central part of Saudi Arabia, at the flowering stage in March 2011. The identification of the plant species was confirmed by a plant taxonomist in the Herbarium Division, College of Science, King Saud University, Riyadh, KSA. A voucher specimen of the plant material was maintained in our laboratory and the herbarium division of King Saud University with voucher specimen no. KSU-3634.

Extraction and isolation of the active anticorrosive phytoconstituent

Shade air-dried and powdered whole plant materials (3.5 kg) of *A. pseudocotula* were first defatted with *n*-hexane three times at room temperature for 72 h each. Then, the defatted plant materials were extracted three times with methanol followed by methanol:water (85:15) three times and finally with water two times at room temperature for 72 hours each. The combined methanolic, aqueous methanolic (mixture) and water extracts were separately concentrated in vacuum at 40 °C until solvents were completely removed. The resultant methanolic (350.0 g), aqueous methanolic (157.0 g) and water (127.0 g) extracts were tested for their anticorrosive properties. The corrosion inhibitive study shows that the methanolic extract has the highest inhibitive effect; hence, it was dissolved in distilled water and successively partitioned with *n*-hexane, chloroform, ethyl acetate and *n*-butanol, which was saturated with water, to give soluble fractions of *n*-hexane (193.0 g), chloroform (15.0 g), ethyl acetate (35.3 g) and *n*-butanol (36.6 g), which were subsequently tested for their anticorrosive properties. The corrosion inhibitive study shows that the *n*-butanol (36.6 g) fraction has the highest inhibitive effect; thus, it was chromatographed over a silica gel (60-120 mesh, 1100 gm) column, and gradient elution was applied with $CHCl_3$:MeOH, where the ratios were 100:0, 80:20, 78:22, 76:24, 74:26, and 70:30. In total, 69 fractions (500 mL each) were collected, their TLC profiles were verified on pre-coated silica gel 60 F254 (0.2 mm, Merck) plates, and their spots were detected using a CAMAG viewing chamber, which was fitted with a UV lamp. Similar fractions were pooled

together based on their TLC profiles as: Fr(s) 14–27 (AP-1), Fr(s) 30-37 (AP-2), Fr(s) 50-55 (AP-3), Fr(s) 58-69 (AP-4). Among all of the pooled fractions, fraction AP-3 has the most potent anticorrosive activity for mild steel in acidic media. The TLC profile of the active subfraction AP-3 shows that this subfraction contains a flavonoidal compound as the major constituent (>90 %). To purify this major compound, subfraction AP-3 was subjected to crystallization in methanol at room temperature, which isolated a pure potent anticorrosive agent **APB**.

Physical and spectroscopic analysis of the isolated compounds

The melting points were determined on a Gallenkamp melting point apparatus and were uncorrected. NMR spectra (1D and 2D) were recorded with a JEOL ECP-400 spectrometer. The NMR samples were prepared in deuterated dimethyl sulfoxide-d_6 (DMSO-d_6) with tetramethylsilane (TMS) as an internal standard. The chemical shifts and coupling constants (J) are expressed in δ (ppm) and Hz, respectively. UV spectra were recorded using a Shimadzu-UV-260 spectrophotometer; λ_{max} (log ε) was measured in nm. MS spectra were recorded on Waters Acquity UPLC-MS/MS, which was equipped with a TQD detector. The samples were infused as a methanol-water solution using API-ESI ionization in either positive or negative mode.

Chemical structure characterization of APB

Luteolin-7-O-*β*-D-glucoside (APB):[25] $C_{21}H_{20}O_{11}$; Yellow amorphous powder, m.p. 255 ℃. ESI-MS (negative mode) m/z: 447 $[M-H]^-$. UV (λ_{max} in MeOH): gives bands at 256 and 348 nm, addition of NaOMe; 263 and 398, NaOAc; 257 and 351, NaOAC-H_3BO_3; 257 and 353, $AlCl_3$; 273, 428 while $AlCl_3$ - HCl; 273, 389. ^{1}H-NMR (400 MHz, DMSO-d_6) δ (ppm): δ 9.92 (1H, brs, 3'-OH), 9.34 (1H, brs, 4'-OH), 7.42 (1H, dd, J = 8.5, 2.5 Hz, H-6'), 7.38 (1H, d, J = 2.5 Hz, H-2'), 6.87 (1H, d, J = 8.5 Hz, H-5'), 6.75 (1H, d, J = 2.5 Hz, H-8), 6.71 (1H, s, H-3), 6.41 (1H, d, J = 2.5 Hz, H-6), 5.04 (1H, d, J = 7.5, H-1''), 3.68 (1H, dd, J = 11.5, 3.5 Hz, H-6''a), 3.45 (1H, dd, J = 11.5, 6.0 Hz, H-6''b), 3.41 (1H, m, H-5''), 3.27 (1H, m, H-3''), 3.25 (1H, m, H-2''), 3.14 (1H, m, H-4''). ^{13}C-NMR (100 MHz, DMSO-d_6) δ (ppm): δ 182.4 (s, C-4), 165.0 (s, C-2), 163.5(s, C-7), 161.7 (s, C-5), 157.5 (s, C-9), 150.5 (s, C-4'), 146.3 (s, C-3'), 122.0 (s, C-1'), 119.7 (d, C-6'), 116.5 (d, C-5'), 114.11(d, C-2'), 105.9 (s, C-10), 103.7 (d, C-3), 100.5 (d, C-1''), 100.1 (d, C-6), 95.3 (d, C-8), 77.7 (d, C-5''), 76.9 (d, C-3''), 73.7 (d, C-2''), 70.1 (d, C-4''), 61.2 (t, C-6'').

Materials, preparation of test specimen and solutions

The working electrode was composed of mild steel, which was purchased from Goodfellow, England, with the following chemical composition (wt %): C-0.2 %, Mn-0.94 %, Si-0.3 %, and the remainder was iron with an uncovered region of 0.9498 cm^2. The uncovered region was mechanically rubbed with several emery papers of different grades, starting with a rough grade paper (600) and continuing in steps to the smoothest (1000) grade. Then, the sample was washed exhaustively with distilled water and finally with acetone to remove all greasy material immediately before insertion in the cell. All chemicals and reagents were of analytical grade, and distilled water was used to prepare the solutions. The aggressive solution of 1.0 M HCl was prepared by diluting AR grade 37 % HCl with distilled water. The appropriate amount of dried extracts of *A. pseudocotula* and pure compound was used to prepare the inhibitor test solutions.

Weight loss measurements

First, the mild-steel specimens were rubbed with sequences of emery paper (grade 600-800-1000), washed with distilled water, degreased with acetone, and dried with an air blower before the weight loss measurement. After they were accurately weighed on an analytical balance with an accuracy of 0.1 mg. , Mild steel specimens were completely immersed in an open beaker, which contained 100 mL of 1.0 M HCl with and without various concentrations of inhibitor at different temperatures (298, 313 and 328±1 K) for 3 h. Then, the mild steel samples were removed, washed with distilled water, completely dried using an air blower and accurately weighed. The inhibitor concentrations of 0.115-0.446 mM were used. All experiments were done in triplicate and results are mentioned from the average of three runs. The percentage inhibition efficiency (IE %) and degree of surface coverage (θ) were determined using the following equations:

$$IE\ \% = \frac{W_0 - W_i}{W_0} \times 100 \qquad (1)$$

$$\theta = \frac{IE\ \%}{100} \qquad (2)$$

where W_0 and W_i are the weight loss of the mild-steel specimens without and with the inhibitors, respectively.

The corrosion rate (C_R) of mild steel was calculated using equation (3):

$$C_R(mm\ year^{-1}) = \frac{87.6\ W}{AtD} \qquad (3)$$

where W is the weight loss of mild steel (mg), A is the area of the specimen, t is the exposure time (h), and D is the density of mild steel (gcm^{-3}).

Electrochemical studies

The electrochemical studies were performed in a conventional three-electrode cell assembly at room temperature using a standard potentiostat, which was equipped with an impedance spectra analyzer. A platinum foil was used as the counter electrode (CE), and a saturated calomel electrode (SCE) that was coupled to a fine Luggin capillary was used as the reference electrode. Prior to the electrochemical measurements, the working electrode was immersed in the test solution for approximately 30 min until a steady open-circuit potential (OCP) was attained. The Tafel plots were recorded from a cathodic potential of −250 mV to an anodic potential of +250 mV at a constant sweep rate of 1 mV/s to examine the effect of green inhibitors on mild-steel corrosion. The linear Tafel segments of the anodic and cathodic curves were extrapolated to the corrosion potential to acquire the corrosion current densities (I_{corr}). The inhibition efficiency was calculated from the measured (I_{corr}) values using equation (4):

$$IE\ \% = \frac{I^0_{corr} - I^i_{corr}}{I^0_{corr}} \times 100 \qquad (4)$$

where I^i_{corr} and I^0_{corr} are the corrosion current densities in the presence and absence of the inhibitor, respectively.

The linear polarization resistance (LPR) R_p was measured by polarizing the specimen from −25 to +25 mV with respect to the corrosion potential (E_{corr}) at a scanning rate of 0.125 mV/s. From the measured polarization resistance value, the inhibition efficiency was calculated using the equation:

$$IE\ \% = \frac{R^i_p - R^0_p}{R^i_p} \times 100 \qquad (5)$$

where R^i_p and R^0_p are the polarization resistances with and without the inhibitor, respectively.

Electrochemical impedance spectroscopy (EIS) measurements were performed at an open circuit potential (OCP) using AC signals of 10 mV amplitude in a frequency range of 30 kHz to 10 mHz. The charge transfer resistance values were obtained from the diameter of the semicircles of the Nyquist plots. The electrical equivalent circuit for the system is shown in Fig. 1. In the given electrical equivalent circuit, R_{ct} is the charge transfer resistance, R_s is the solution resistance, and C_{dl} is the double-layer capacitance. The inhibition efficiencies of the inhibitors were calculated from the charge transfer resistance values using equation (6):

$$IE\ \% = \frac{R^i_{ct} - R^0_{ct}}{R^i_{ct}} \times 100 \qquad (6)$$

where R^0_{ct} and R^i_{ct} are the charge transfer resistances without and with the inhibitor, respectively.

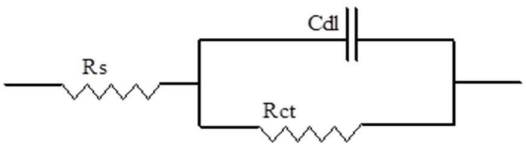

Fig. 1 The electrical equivalent circuit for AC impedance measurement.

SEM and EDS analysis

The mild steel specimens were dipped in 100 mL of 1.0 M HCl without and with the green inhibitor concentration of 0.446 mM for 3 h. Then, they were retrieved, immediately rinsed with acetone and maintained at room temperature until they were completely dried. The surface morphology of the specimens was examined using a JEOL–JSM-6380LA Scanning Electron Microscope (SEM–EDS).

Stability test of phytomolecule APB in 1.0 M HCl medium

The isolated active phytomolecule **APB** (100 mg) was dissolved in 1.0 M HCl solution and kept at room temperature for 48 hours. After 48 hours the acidic solution of **APB** was neutralized by sodium bicarbonate and filtered. The filtered neutral solution was extracted with water saturated *n*-butanol. *n*-butanol extract was dried completely in vacuum at 40 °C until solvents were completely removed to give yellow color amorphous powder. A part of this compound was dissolved in methanol and Co-TLC was checked with pure **APB**. Both compounds showed the same R_f value suggesting that **APB** was stable in 1.0 M HCl medium. Moreover, NMR data of both compounds were also found to be same suggesting that **APB** was stable in tested corrosive medium.

Results and discussion

As part of our interest in the phytochemical investigations of plants in Saudi Arabia,[18,19,26,27] we present a detailed study of the

anticorrosive properties of different extracts (methanolic, aqueous methanolic and water extracts) of *A. pseudocotula* for mild steel in 1.0 M HCl media using Tafel plots measurements, linear polarization measurements and electrochemical impedance spectroscopic (EIS) methods. Typical cathodic and anodic polarization curves of mild steel in 1.0 M HCl solution without and with 600 ppm of methanolic, aqueous methanolic and water extracts are shown in Fig. S9 of the supporting information and their electrochemical parameters are provided in Table S1 of the supporting information.

The inhibition efficiencies obtained from Tafel plots and linear polarization measurements were calculated from the acquired I_{corr} and R_p values using equations 4 and 5, respectively. In addition, Fig. S10 of the supporting information shows the results of the electrochemical impedance spectroscopic (EIS) measurements of mild steel in a 1.0 M HCl solution without and with 600 ppm of methanolic, aqueous methanolic and water extracts in the form of Nyquist plots. The impedance parameters acquired from the Nyquist plots are shown in Table S2 of the supporting information. The inhibition efficiency values were calculated using equation 6.

These results show that all three extracts of *A. pseudocotula* show good to significant corrosion inhibitive properties for mild steel in acidic media with inhibition efficiencies of 75-87%. However, among these three extracts, the methanolic extract shows the highest corrosion inhibition efficiency; thus, it was selected to isolate the active anticorrosive agent. The methanolic extract was dissolved in distilled water and fractionated with *n*-hexane, chloroform, ethyl acetate and finally *n*-butanol that was saturated with water. Only the ethyl acetate and *n*-butanol fractions were tested for their anticorrosive properties because the *n*-hexane and chloroform fractions were not soluble in 1.0 M HCl solutions.

The results obtained from Tafel plots and EIS measurements for ethyl acetate and *n*-butanol fractions are shown in Figs. S11 and S12 of the supporting information, respectively, whereas their respective electrochemical parameters are provided in Tables S3 and S4 of the supporting information. Both fractions show promising anticorrosive properties for mild steel in acidic media with inhibition efficiencies of 83 % and 87 %, respectively. Nevertheless, the *n*-butanol fraction is more active than the ethyl acetate fraction (Fig. 2).

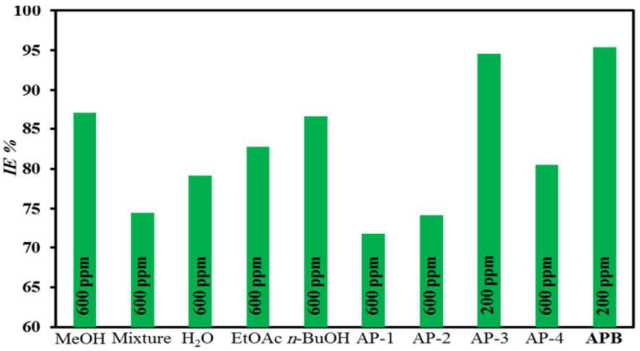

Fig. 2 Corrosion inhibitive effects of various extracts, fractions and purified compound of *A. pseudocotula* for mild steel in 1.0 M HCl solution.

Therefore, the *n*-butanol fraction was selected for the isolation and identification of its active anticorrosive agent. For this purpose, the *n*-butanol fraction was subjected to column chromatographic separation on silica gel using chloroform and various proportions of chloroform and methanol mixtures as the eluting solvents. In total, 81 fractions were collected and pooled together based on their TLC profiles, which furnished four subfractions: AP-1 to AP-4. All of the pooled subfractions (AP-1 to AP-4) were tested for their anticorrosive activity for mild steel in 1.0 M HCl medium. The potentiodynamic polarization measurement results are shown in Fig. S13 of the supporting information in the form of polarization curves, and their electrochemical parameters are provided in Table S5 of the supporting information. The results from the electrochemical impedance spectroscopic (EIS) methods are shown in Fig. S14 of the supporting information in the form of Nyquist plots, and their electrochemical parameters are mentioned in Table S6 of the supporting information.

These results evidently show that subfraction AP-3 exhibits the most potent anticorrosive properties with a 95% inhibition efficiency even at notably low concentrations compared to other subfractions (Fig. 2). The TLC profile of the active subfraction AP-3 shows that it contains a flavonoidal compound as the major constituent (>90%). To purify this major compound, subfraction AP-3 was subjected to crystallization in methanol at room temperature, which yielded the pure compound **APB**.

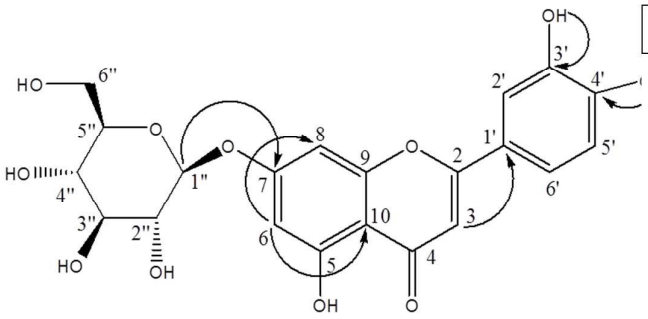

Fig. 3 Chemical structure and key HMBC (→) correlations of compound **APB**.

Compound **APB** was identified as luteolin-7-O-β-D-glucoside (Fig. 3) using various spectroscopic techniques, such as 1D and 2D NMR (^{1}H and ^{13}C-NMR, DEPT, COSY, HMQC, HSQC, NOESY and HMBC) (Supporting information, Figs. S1-S8). Moreover, its anticorrosive properties on mild steel in 1.0 M HCl aggressive media were evaluated in details using the weight loss, Tafel plots, linear polarization, electrochemical impedance spectroscopic (EIS), and SEM and EDS methods.

3.1 Weight loss study

The effect of different concentrations of compound **APB** on the inhibition efficiency of mild steel in 1.0 M HCl was studied using a weight loss experiment at 298±1 K for an immersion period of 3 h. The percentage inhibition efficiency (IE %), corrosion rate and surface coverage (θ) obtained from this method are summarized in Table 1, whereas Fig. 4 shows the effect of the inhibitor concentrations on the inhibition efficiency of mild steel in 1.0 M HCl solution.

Table 1

Inhibition efficiency, weight loss, surface coverage and corrosion rate at different **APB** concentrations for mild-steel corrosion in 1.0 M HCl from weight loss measurements at 298±1 K.

Concentration of inhibitor (mM)	Weight loss (g)	Surface coverage (θ)	Corrosion rate $C_R(mm\ year^{-1})$	IE %
0 (Blank)	0.2587	-	0.1327	-
0.112	0.0227	0.91	0.0119	91.2 ±0.37
0.223	0.0166	0.94	0.0087	93.6 ± 0.86
0.335	0.0151	0.94	0.0079	94.2 ± 0.11
0.446	0.0134	0.95	0.0070	94.8 ± 0.35
0.558	0.0133	0.95	0.0069	94.9 ± 0.61

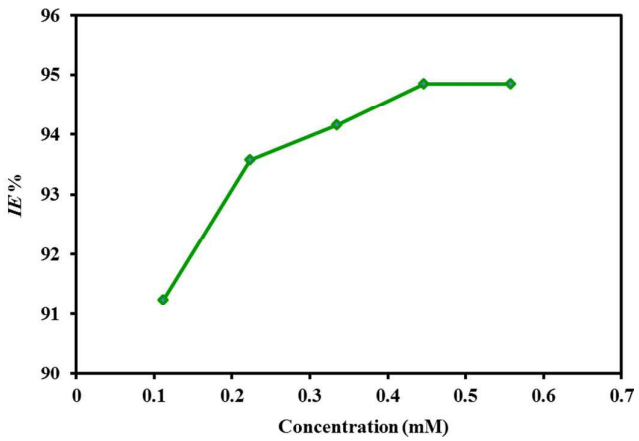

Fig. 4 Variation of the inhibition efficiency with various concentrations of **APB**.

Table 1 and Fig. 4 clearly show that the inhibition efficiency increases with the increase in inhibitor concentration in a 1.0 M HCl solution, which suggests that the number of inhibitor molecules that is adsorbed over the surface of mild steel increases. Thus, the inhibitor molecules cover more area of the active sites of mild steel where direct acid attack occurs and protect mild steel against corrosion.[16] The highest inhibition efficiency is obtained at a concentration of 0.446 mM. Further increases in the inhibitor concentration do not significantly change the protective effect of the green inhibitor (Fig. 4). Therefore, 0.446 mM was considered to be the optimal concentration for this green inhibitor **APB**. After the optimum inhibitor concentration to achieve maximum inhibition efficiency is determined, the effect of different temperatures (298±1-328±1 K) in the absence and presence of the optimal inhibitor concentration was investigated during 3 h of immersion time, and the results are shown in Table 2 and Fig. 5.

Table 2

Inhibition efficiency, weight loss, surface coverage and corrosion rate at various temperatures for the corrosion of mild steel in 1.0 M HCl in the presence of 0.446 mM of **APB** from the weight loss measurements.

Temperatures (K)	Weight loss (g)	Surface coverage (θ)	Corrosion rate $C_R(mm\ year^{-1})$	IE %
298±1	0.0134	0.95	0.0070	94.8 ± 0.35
313±1	0.0168	0.94	0.0088	93.5 ± 0.40
328±1	0.0217	0.92	0.0114	91.6 ± 0.31

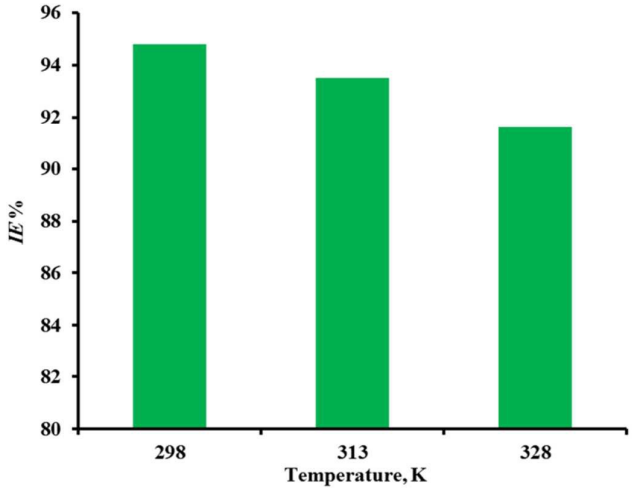

Fig. 5 Variation of the inhibition efficiency in the presence of the optimal concentration (0.446 mM) of **APB** at various solution temperatures.

Table 2 and Fig. 5 show that the inhibition efficiency with the optimal inhibitor concentration decreases when the temperature of the inhibitive solution increases, which indicates that the adsorption mechanism of the inhibitor may involve physisorption instead of chemisorption because physisorption is an electrostatic interaction, which generally loses its effect at elevated temperatures [12].

3.2 Tafel plots measurements

The inhibitive effect of the pure natural compound **APB** was studied using potentiodynamic polarization measurements. Tafel plots of mild steel in a 1.0 M HCl solution without and with several concentrations of **APB** are shown in Fig. 6.

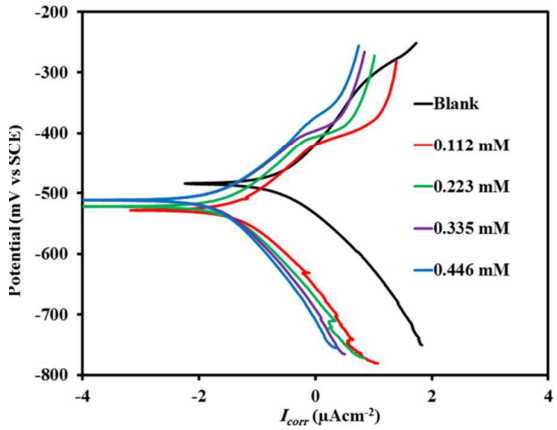

Fig. 6 Tafel plots without and with different concentrations of **APB** in 1.0 M HCl.

Fig. 6 evidently shows that the corrosion current density of the anodic and cathodic curves decreases in the presence of the green inhibitor **APB** compared to that recorded for the blank solution, which indicates corrosion mitigation. This decrease is more pronounced with the increase in concentration of the green corrosion inhibitor, which suggests that an increase in inhibitor concentration leads to an increase in the adsorption of inhibitor molecules at the mild steel/acid solution interface, which provides more surface coverage for the active sites of mild steel where direct acid attack occurs and mitigates the corrosion process.[28] The electrochemical factors, such as the corrosion current density (I_{corr}), anodic (β_a) and cathodic (β_c) Tafel constants, corrosion potential (E_{corr}), polarization resistance (R_p) and inhibition efficiency (IE %), which were obtained from the Tafel plots at the corrosion potential (E_{corr}) and linear polarization measurements, are reported in Table 3.

Table 3 Potentiodynamic polarization parameters obtained from Tafel plots for the corrosion of mild steel in 1.0 M HCl with various concentrations of **APB**.

APB Concentration (mM)	E_{corr} (mV)	I_{corr} (µAcm^{-2})	β_a (mV/dec)	β_c (mV/dec)	R_p	IE % Tafel	IE % LPR
0 (Blank)	−486.6	213.0	99.85	−110.73	54.5	-	-
0.112	−531.5	18.2	71.62	−87.02	579.3	91.5	90.6
0.223	−528.5	15.8	73.78	−94.50	603.0	92.6	91.0
0.335	−520.1	11.3	74.88	−98.44	967.9	94.7	94.4
0.446	−515.9	9.2	76.28	−103.43	1011.5	95.7	94.6

The inhibition efficiency obtained from Tafel plots and linear polarization measurements were calculated from the I_{corr} and R_p values using equations 4 and 5, respectively. Table 3 clearly shows that with the increase in inhibitor concentration, the corrosion current density (I_{corr}) significantly decreases and that its values are much lower than that in the uninhibited acidic solutions. However, because of the inverse association between the corrosion current density (I_{corr}) and the polarization resistance (R_p), the polarization resistance (R_p) tends to significantly increase when the inhibitor concentration increases, which increases the inhibition efficiency, as expected. This result suggests that by increasing the inhibitor concentration, the adsorption amount of phytomolecule on the metal surface also increases, which creates a physical wall for the mass and charge transfer and significantly protects the metal surface by blocking the active sites.[11] Table 3 also shows that the addition of the green inhibitor changes slightly both the anodic Tafel constant (β_a) and the cathodic Tafel constants (β_c), which indicates that the adsorption of green inhibitor does not modify the mechanism of both anodic (metal dissolution) and cathodic (hydrogen evolution)

reactions. Thus, the inhibitor can be classified as a mixed-type inhibitor with slightly more cathodic effectiveness because its addition shifts the values of E_{corr} in the negative direction. However, the shift in E_{corr} values is not prominent, and the maximum displacement in E_{corr} for this natural compound is only 43 mV towards cathodic polarization, which indicates that this inhibitor acts as a mixed-type inhibitor with dominating cathodic effectiveness.[28] Moreover, the results in Fig. 6 also suggest that both anodic and cathodic reactions are inhibited in 1.0 M HCl, but the cathode is more polarized. Hence, the properties of the mixed-type inhibitor with dominant cathodic effect are revealed.

3.3 Electrochemical impedance spectroscopic (EIS) measurements

The corrosion behaviour of mild steel in a 1.0 M HCl solution in the presence of **APB** was examined with EIS at room temperature after an exposure period of 30 min. The Nyquist plots for mild steel acquired at the interface in the absence and presence of various concentrations of **APB** are provided in Fig. 7.

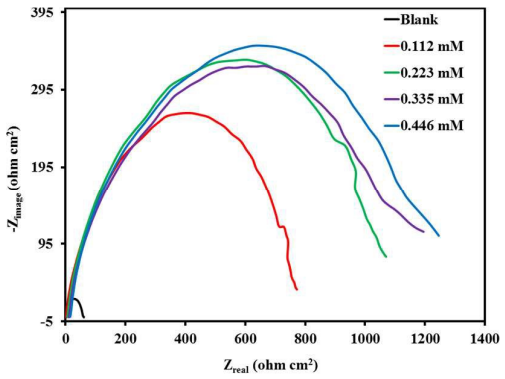

Fig. 7 Nyquist plots without and with various concentrations of **APB** in 1.0 M HCl.

Fig. 7 shows that the impedance behaviour of mild steel was considerably affected by the addition of the green inhibitor in a 1.0 M HCl solution and that the diameter of the Nyquist plots increases with increasing inhibitor concentration. This result suggests that an effective protective layer was developed on the mild steel through the adsorption of phytomolecule and that the developed protective layer was further strengthened when the inhibitor concentration increases, which provides more protection to mild steel in an aggressive medium. Moreover, the Nyquist plots comprise a depressed semi-circle with the centre below the real X-axis; this type of behaviour represents a typical characteristic of solid electrodes and more often alludes to frequency dispersion, which emerges because of the coarseness and unevenness of the solid surface.[29] The impedance parameters (charge transfer resistance (R_{ct}), double-layer capacitance (C_{dl}) and inhibition efficiency (IE %)), which were derived from the Nyquist plots, are shown in Table 4.

Table 4 Electrochemical impedance parameters obtained from the Nyquist plots for the corrosion of mild steel in 1.0 M HCl with various concentrations of **APB**.

Concentration (mM)	R_{ct} (Ω cm^2)	C_{dl} (μF cm^{-2})	θ	IE %
0 (Blank)	57.1	533.0	-	-
0.112	791.1	112.5	0.93	92.8
0.223	1099.0	144.0	0.95	94.8
0.335	1170.0	172.6	0.95	95.1
0.446	1242.0	177.0	0.95	95.4

The inhibition efficiency values were determined using equation 6, whereas the double-layer capacitance (C_{dl}) was determined as follows:

$$C_{dl} = \frac{1}{2\pi f_{max} R_{ct}} \qquad (7)$$

where f_{max} is the frequency at the apex of the Nyquist plots and R_{ct} is the charge transfer resistance. Table 4 shows that the charge transfer resistance (R_{ct}) values of the inhibited substrates increases when the amount of inhibitor increases, which can be interpreted as a result of the formation of an insulating adsorption layer of phytomolecules on the surface of mild steel, which increases the inhibition efficiency (IE %) values.[30] Furthermore, as expected, the double-layer capacitance (C_{dl}) tends to decrease with increasing inhibitor concentration possibly because the thickness of the electrical double layer increases and/or the local dielectric constant decreases, which suggests that this natural compound **APB** acts through adsorption at the mild-steel/solution interface.[29] It may be presumed that C_{dl} decreases because of the progressive replacement of water molecules by the adsorption of **APB** on the mild steel surface, which provides more surface coverage to the active site of mild steel by the inhibitor and decreases the magnitude of the mild steel dissolution and charge transfer.[31] Moreover, the EIS measurements show that this green inhibitor exhibits a promising anticorrosive property for mild steel in 1.0 M HCl with the highest inhibition efficiency of 94% at the concentration of 0.446 mM. The

data acquired from the EIS measurements are consistent with those achieved from the potentiodynamic polarization and weight loss methods (Fig. 8).

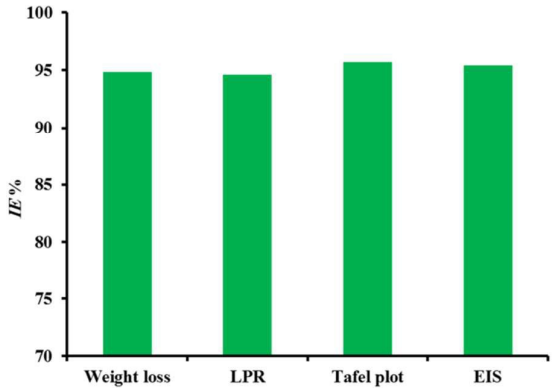

Fig. 8 Inhibition efficiency obtained from various methods in the presence of the optimal concentration of **APB**.

3.4 Adsorption isotherm and inhibition mechanism

The adsorption isotherm provides elementary evidence on the relationship between the corrosion inhibitor and the metal surface. An inhibitor can be considered to be a potent corrosion inhibitor in aqueous solution only when the interaction force between the metals and the inhibitor is greater than the interaction force of the metal and water molecules.[32] The adsorption process of the inhibitor is a replacement of the adsorption process between the organic molecules in the aqueous solution Org(sol) and water molecules H_2O(ads) from the metal surface, which can be represented as:[33]

$$Org(sol) + xH_2O(ads) \leftrightarrows Org(ads) + nH_2O(sol) \quad (8)$$

where Org(sol) and Org(ads) are the organic molecules in aqueous solutions and those adsorbed on the metallic surface, respectively, whereas H_2O(ads) is the water molecules on the metallic surface and x is the number of water molecules replaced by one organic adsorbate molecule.

The most commonly applied adsorption isotherms are Temkin, Langmuir and Frumkin isotherms. According to these isotherms, θ is related to the inhibitor concentration:

$$\log\left(\frac{\theta}{C}\right) = \log K - g\theta \quad \text{(Tempkin isotherm)} \quad (9)$$

$$\frac{C}{\theta} = \frac{1}{K} + C \quad \text{(Langmuir isotherm)} \quad (10)$$

$$\log\left\{\frac{\theta}{(1-\theta)C}\right\} = \log K - g\theta \quad \text{(Frumkin isotherm)} \quad (11)$$

where θ is the surface coverage, K is the adsorption-desorption equilibrium constant, C is the concentration of inhibitor, and g is the adsorbate parameter.

Using the surface coverage (θ) values that correspond to different concentrations of inhibitor at 298±1 K, attempts were made to fit several adsorption isotherms such as Langmuir, Temkim and Frumkin isotherms. However, the best fit was obtained with the Langmuir isotherm, which gives a straight line with a unit slope, and the regression coefficient r^2 is 0.9999 for **APB** (Fig. 9).

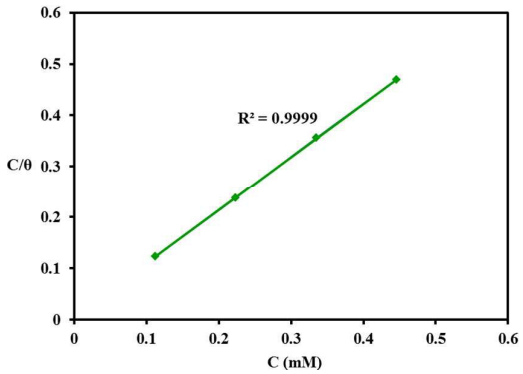

Fig. 9 Langmuir isotherm in the presence of different concentrations of **APB** in 1.0 M HCl.

This result suggests that the Langmuir isotherm displays the best correlation with the experimental data, which indicates the monolayer formation of the inhibitor on the surface of mild steel.[34]

The free energy of adsorption process ΔG°_{ads} was calculated using the following equation:

$$\Delta G^{\circ}_{ads} = -RT\ln(K \times 55.5) \quad (12)$$

where K is the equilibrium constant of the adsorption process. Generally, ΔG°_{ads} of approximately -20 kJ mol^{-1} or less negative indicates an electrostatic interaction between the charged molecules and the charged metal (physisorption), whereas values of approximately -40 kJ mol^{-1} or higher indicate charge sharing or charge transfer from the organic compounds to the metal surface to form a coordinate type of bond (chemisorption).[35] The calculated ΔG°_{ads} from the Langmuir adsorption isotherm in this study is -39.64 kJ mol^{-1} (Table 5). The value of ΔG°_{ads} indicates that **APB** is adsorbed on the MS surface by a combination of both physisorption and chemisorptions. More negative value of ΔG°_{ads} indicates a stronger interaction between the inhibitor molecules and the metal surface. Moreover, in weight loss study inhibition efficiency (IE %) was observed to decrease when the temperature of the inhibition solution increased. This indicates that **APB** molecules are adsorbed physically to the MS surface while chemisorption has the minor contribution in the adsorption process.[36] When the temperature

increases, the number of adsorbed molecules on the metal surface decreases, which decreases the inhibition efficiency (IE %).[10] The other thermodynamic parameters, such as the enthalpy and entropy of adsorption, were calculated from the following equations:

$$\Delta H^{\circ}_{ads} = E_a - RT \quad (13)$$

$$ln\ C_R = ln\ A - \frac{E_a}{RT} \quad (14)$$

$$\Delta G^{\circ}_{ads} = \Delta H^{\circ}_{ads} - T\Delta S^{\circ}_{ads} \quad (15)$$

where ΔH°_{ads} and ΔS°_{ads} are the enthalpy and entropy of adsorption, respectively. The obtained results are shown in Table 5, where the negative sign of ΔH°_{ads} indicates that the adsorption of inhibitor on the MS surface is exothermic.[11]

Table 5

Thermodynamic parameters for mild steel in 1.0 M HCl in the presence of an optimal concentration 0.446 mM of the green inhibitor **APB**.

Compound	ΔG°_{ads} (kJmol^{-1})	ΔH°_{ads} (kJmol^{-1})	ΔS°_{ads} (JK^{-1})
APB	−39.64	−10.71	−97.08

3.5 SEM and EDS analysis

The surface analysis of metals using scanning electron microscope (SEM) images has become an essential tool to study the surface morphology of corroded and uncorroded metals.[11] To confirm the interaction of the inhibitor with the mild steel surface, SEM images were recorded for mild-steel samples in the absence and presence of the optimal inhibitor concentration. The results are shown in Fig. 10.

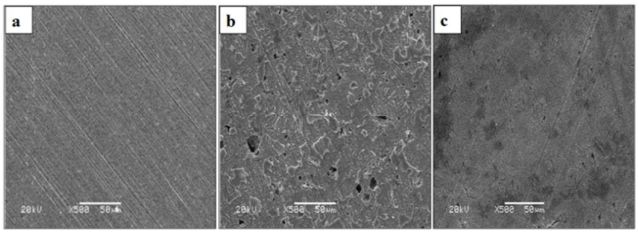

Fig. 10 SEM images of (a) polished mild-steel coupon, (b) mild-steel coupon in 1.0 M HCl and (c) mild-steel coupon with 0.446 mM of **APB** in 1.0 M HCl.

Fig. 10a shows the SEM image of a freshly abraded mild-steel sample without treatment. Fig. 10a indicates a notably smooth surface of mild steel with some minor scratches, which might have arisen during abrasion. Fig. 10b shows the image of the mild steel sample that was treated in 1.0 M HCl for 3 hr. Here, the mild-steel surface was rigorously corroded because of the aggressive attack of 1.0 M HCl. Fig. 10c shows the SEM image of mild steel that was treated with an optimal concentration of inhibitor (0.446 mM) in 1.0 M HCl for 3 hr. In this figure, a notably smooth mild steel surface is observed, which is notably comparable with the polished mild-steel surface (cf. Fig. 10a). This result indicates that a protective film was formed by the inhibitor molecules on the mild-steel surface, which significantly inhibits the corrosion of mild steel in the 1.0 M HCl solution.[11]

The energy dispersive spectrometry (EDS) analysis of mild-steel samples in the absence and presence of optimal inhibitor concentration was performed to determine the percentage of chloride content on the surface of mild steel. The obtained results are shown in Fig. 11.

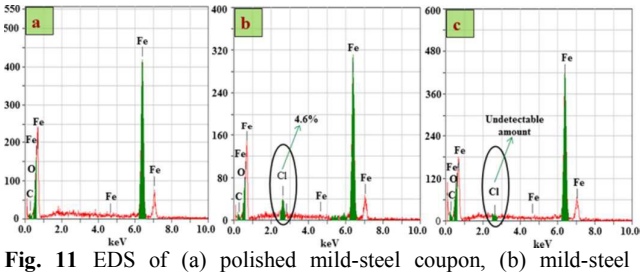

Fig. 11 EDS of (a) polished mild-steel coupon, (b) mild-steel coupon in 1.0 M HCl and (c) mild-steel coupon with 0.446 mM of **APB** in 1.0 M HCl.

Fig. 11a shows the EDS results of the polished mild-steel sample, which shows that the polished mild-steel surface is chlorine free. Fig. 11b shows the results of the mild-steel sample that was treated in 1.0 M HCl solution for 3 hr, where chlorine was detected in significant amount (4.6%) on the surface of mild steel because of the aggressive attack of the 1.0 M HCl solution. Fig. 11c shows the spectrum of mild steel that was treated with an optimal inhibitor concentration (0.446 mM) in 1.0 M HCl for 3 hr. This spectrum shows a negligible amount of chloride ions on the surface of mild steel that was treated with **APB** in 1.0 M HCl solution. Thus, this green inhibitor efficiently protects mild steel from corrosive solution.[11]

Conclusions

In this study, we screened, for the first time, the anticorrosive properties of various extracts of *A. pseudocotula* for mild steel in 1.0 M HCl media using different electrochemical techniques. Among various extracts of *A. pseudocotula*, the methanolic extract showed the highest corrosion inhibition activity. The anticorrosive assay-guided fractionation and isolation of this active extract resulted in the isolation of a highly potent anticorrosive natural compound **APB**. The isolated active molecule **APB** was identified as luteolin-7-O-*β*-D-glucoside based on several spectroscopic analyses. Detailed study on the anticorrosive effects of this compound using weight loss, Tafel extrapolation, linear polarization, electrochemical impedance

spectroscopy (EIS) and SEM and EDS techniques revealed that this natural compound remarkably inhibits the corrosion of mild steel in acidic solution and that the inhibition efficiencies increase when the concentration of **APB** increases. Electrochemical studies proved that this natural compound acts as a mixed-type inhibitor with dominating cathodic effect. The adsorption behaviour of the green inhibitor on the mild steel surface, according to the Langmuir adsorption isotherm and adsorption process, is spontaneous, exothermic and corresponds to physical adsorption. Moreover, the surface morphology study using a scanning electron microscope (SEM) and energy dispersive spectrometry (EDS) analysis showed a substantial improvement in surface morphology of the mild-steel plate with the green inhibitor in the 1.0 M HCl media. The results of the electrochemical tests and weight loss measurements are consistent and show that this green inhibitor, which was isolated from the methanolic extract of *A. pseudocotula*, can be potentially applied as an anticorrosive agent for mild steel in hydrochloric acid environment.

Acknowledgements

This project was supported by King Saud University, Deanship of Scientific Research, College of Science, Research Center.

Notes and references

1 H. H. Uhlig, R. W. Revie, Corrosion and corrosion control. John Wiley, New York, 1985.
2 D. A. Jones, Principles and Prevention of Corrosion, Macmillan, New York, 1992.
3 M. W. Ranney, Inhibitors—Manufacture and Technology, Noyes Data Corp, New Jersey, 1976.
4 S. A. Abd El-Maksoud, *J. Electroanal. Chem.* 2004, **565**, 321-328.
5 J. J. Fu, H. S. Zang, Y. Wang, S. N. Li, T. Chen, X. D. Liu, *Ind. Eng. Chem. Res.* 2012, **51**, 6377–6386.
6 P. B. Raja, M. G. Sethuraman, *Mat. Lett.* 2008, **62**, 113–116.
7 M. A. Quraishi, A. Singh, V. K. Singh, D. K. Yadav, A. K. Singh, *Mat. Chem. Physics* 2010, **122**, 114–122.
8 M. A. Ameer, A. M. Fekry, *Prog. Org. Coat.* 2011, **71**, 343–349.
9 L. R. Chauhan, G. Gunasekaran, *Corros. Sci.,* 2007, **49**, 1143–1161.
10 M. H. Hussin, M. J. Kassim, *Mat. Chem. Phys.,* 2011, **125**, 461–468.
11 M. Gopiraman, P. Sakunthala, D. Kesavan, V. Alexramani, I. S. Kim, N. Sulochana, *J. Coat. Technol. Res.* 2012, 9, 15–26.
12 A. Y. El-Etre, *Mater. Chem. Phys.,* 2008, 108, 278-282.
13 P. C. Okafor, M. E. Ikpi, I. E. Uwaha, E. E. Ebenso, U. J. Ekpe, S. A. Umoren, *Corros. Sci.,* 2008, 50, 2310–2317.
14 H. Cang, Z. Fei, H. Xiao, J. Huang, Q. Xu, Int. *J. Electrochem. Sci.*, 2012, **7**, 8869–8882.
15 P. Sakunthala, S. S. Vivekananthan, M. Gopiraman, N. Sulochana, A. R. Vincent, *J. Surfact. Deterg.,* In press, DOI 10.1007/s11743-012-1405-5.
16 P. B. Raja, M. G. *Mat. Corros.* 2009, **60**, 22-28.
17 H. Gerengi, H. I. Sahin, *Ind. Eng. Chem. Res.,* 2012, 51, 780–787.
18 M. Khan, A. A. Mousa, K. V. Syamasundar, H. Z. Alkhathlan. *Nat. Prod. Commun.,* 2012, **7**, 1079–1082.
19 M. S. Al-Otaibi, A. M. Al-Mayouf, M. Khan, A. A. Mousa, S. A. Al-Mazroa, H. Z. Alkhathlan, *Arabian J. Chem.* 2014, **7**, 340-346.
20 C. Oberprieler, *Taxon*, 2001, **50**, 745-762.
21 A. Ghafoor, T. A. Al-Turki, *Edinburgh J. Bot.,* 1999, **56**, 55-59.
22 J. Thomas, Herbarium (KSU): Dept. of Botany & Microbiology, King Saud University, Riyadh, Saudi Arabia. Available: http://www.plantdiversityofsaudiarabia.info/Biodiversity-Saudi-Arabia/Flora/Widely%20distributed/Widely%20Distributed%20species.htm [accessed 1st April 2013].
23 S. Collenette, *An illustrated guide to the flowers of Saudi Arabia*, Flora publication No. 1, Scorpion Publishing Ltd, Buckhurst hill, Essex, (1985) pp. 137.
24 A. Migahid, M. Hammouda, *Flora of Saudi Arabia,* Vol ***I***. Riyadh University Publication, Riyadh, (1978) p. 620.
25 U. Ozgen, H. Sevindik, C. Kazaz, D. Yigit, A. Kandemir, H. Secen, I. Calis, *Molecules*, 2010, **15**, 2593-2599.
26 H. Z. Alkhathlan, M. Khan, M. M. S. Abdullah, A. M. Al-Mayouf, A. A.Mousa, Z. A. M. Al-Othman. *Int. J. Electrochem. Sci.,* 2014, **9**, 870-889.
27 M. Khan, M. A. Al-Mansour, A. A. Mousa, and H. Z. Alkhathlan. *J. Essent.Oil Res.,* 2014, **26**,13-18.
28 I. Ahmad, R. Prasad, M. A. Quraishi, Corros. Sci., 2010, **52**, 1472–1481.

29 M. Elayyachy, A. El Idrissi, B. Hammouti, *Corros. Sci.,* 2006, **48**, 2470–2479.

30 K. F. Khaled, M. M. Al-Qahtani, *Mater. Chem. Phys.,* 2009, **113**, 150.

31 F. Bentiss, B. Mehdi, B. Mernari, M. Traisnel, H. Vezin, Corrosion, 2002, **58**, 399-407.

32 V. S. Sastri, E. Ghali, M. Elboujdaini, Corrosion prevention and protection: Practical solutions, John Wiley & Sons Ltd., 2007, p. 84.

33 K. Tebbji, B. Hammouti, H. Oudda, A. Ramdai, M. Benkadour, Appl. Surf. Sci., 2005, 252, 1378-1385.

34 S. Cheng, S. Chen, T. Liu, X. Chang, Y. Yin, *Mater. Lett.,* 2007, 61, 3276-3280.

35 A. Yurt, S. Ulutas, H. Dal, *Appl. Surf. Sci.,* 2006, **253,** 919-925.

36 M. Ozcan, J. Solid State Electrochem., 2008, 12, 1653–1661.